



## Correspondence and difference between gamma-ray and neutron irradiation effects on organic materials in marine environment

Elsayed K. Elmaghraby<sup>1</sup>, Saad Abdelaal<sup>2,3</sup>, Abdelwahab M. Abdelhady<sup>2,3</sup>,  
Samar Fares<sup>4\*</sup>, Safwat Salama<sup>5</sup>, Nassif A. Mansour<sup>6</sup>

- 1- Experimental Nuclear Physics Department, Nuclear Research Center, Atomic Energy Authority, Cairo 13759, Egypt.
- 2- Accelerator and ion sources Department, Nuclear Research Center, Atomic Energy Authority, Cairo 13759, Egypt.
- 3- Central Lab for Elemental & Isotopic Analysis, Nuclear Research Center, Cairo, Egypt.
- 4- Basic Science Department, Zagazig Higher Institute of Engineering and Technology, Zagazig, Egypt.
- 5- Radiation Protection Department, Nuclear Research Center, Atomic Energy Authority, Egypt.
- 6- Physics Department, Faculty of Science, Zagazig University, Egypt.

\*Corresponding author: [sf.samar@yahoo.com](mailto:sf.samar@yahoo.com)

### ARTICLE INFO

#### Article History:

Received: Nov. 2, 2019

Accepted: Nov. 28, 2019

Online: Nov. 30, 2019

#### Keywords:

Marine life  
Environment  
PADC polymer (CR-39)  
Neutron  
gamma rays  
Physico-chemical analysis  
FTIR spectroscopy

### ABSTRACT

This work is devoted to understand the difference between gamma ray effects and neutron influence on organic materials in order to interpret the change occurred in organic matter that coexists with nuclear tests in deep marine environment. A combination of Fourier-transform infrared spectroscopy (FTIR) and a simple statistical analysis was applied as a tool for the quantitative determination of changes in chemical properties due to radiation effects. The primary goal of this work was to statistically deduce, from correlations obtained between different band intensities, more information on the changes occurred. It did not aim only to investigate in detail the PolyAllyl Diglycol Carbonate (PADC) structure due to gamma and neutron irradiation impacts. The PADC samples obtained from Track Analysis System Ltd., UK of TASTRAK type were irradiated with gamma-ray dose in the range from  $(5\pm 1)\times 10^3$  Gy to  $(3.0\pm 0.6)\times 10^6$  Gy using  $^{60}\text{Co}$  standard gamma cell of calibrated dose rate. While a high neutron fluence from ETRR-2 research reactor was applied for neutron irradiation process. The results showed a shift in absorption intensities for various bands due to either gamma or neutron irradiation. Such bands are the C=O, C=C and C-O-C. Moreover, formation of -OH radical was observed which indicating water content in the studied samples after irradiation. Such induced alterations were due to bond breakage of weak bonds such as, C-H, C-O, and C-C with different possibilities for gamma irradiation effects. While for neutron irradiation, atomic displacement in the material was the main reason for such changes. Furthermore, by applying a simple statistical analysis test, major infrared bands were integrated in order to make sense of, and draw correlations between each other to get more accurate and comparable results. The obtained results showed a good correlation between some bands, while the other didn't. Also, the applied correlations simplified the comparison between gamma ray and neutron induced effects.

### INTRODUCTION

Organic materials that exist in marine environment may have clues about the radioactivity they exposed to. Natural and anthropogenic radionuclides are abundant in the marine biosphere which includes uranium, thorium, and potassium activities (Mee and Readman, 1993; Claudia *et al.*, 2018).

They are used to study a suite of environmental processes, including those related to marine food webs, yet they also potentially negatively impact marine biota and humans. These sources of radioactivity are gamma emitters; nuclear experiments that may be performed in deep marine environments, expose the organic materials to intense neutron fields (Právělie, 2014). These neutrons had a local isotopic signature of increasing the  $^{14}\text{C}$  contents in the solid rocks. Its effect on other organic material that exists in the time of the test may represent another evidence.

The act of radiation on polymeric materials is of great concern to execute several desirable improvements in polymer properties that cannot be attained by chemical ways (Kumar and Singh, 2013; Sangeeta Prasher *et al.*, 2015). It is in addition beneficial to examine the modification in the physical, chemical, structural, mechanical, optical, and surface properties of polymer due to irradiation (Zaki *et al.*, 2016). In what way, the impact of these changes occurred depends on the structural formation of the polymer substantially as the irradiation conditions such as energy, fluence as well as LET (Linear Energy Transfer) of the radiation (Sahoo *et al.*, 2014; Sangeeta Prasher *et al.*, 2015). The advantageous properties of these materials made it needed in a wide range of applications. CR-39 polymer detector, which is the brand name of Poly allyl Diglycol Carbonate (PADC), is one of these polymeric materials (Zaki and Elmaghraby, 2008; Saad *et al.*, 2018). It is a thermoset homo-polymer commonly used as a solid-state nuclear track detector (SSNTD) in different disciplines, such as nuclear reaction physics, neutron dosimetry and radiobiological measurements (El-Badry *et al.*, 2009; Saad *et al.*, 2012).

For more informative from a scientific point of view, a great attention has been paid to investigate defects and modifications of PADC for such applications. This involves both knowing and understanding of irradiation defect and how they affect material properties (Abdul-Kader *et al.*, 2014).

In polymeric materials, neutrons may cause different effects compared to gamma-rays released the same dose because of their high linear energy transfer (Bo Liu *et al.*, 2017). Neutron irradiation does not cause ionization directly in the material. However, the inquisitive part lies in the secondary impacts due to recoiling nuclei of the detector under neutron fluence, leading to charged particles production that cause ionization (Castillo *et al.*, 2013). Whilst, gamma rays indirectly ionize the target polymer through energetic secondary electrons which produced through photoelectric effect, Compton scattering and pair production processes (Siddhartha *et al.*, 2012; Kulwinder Singh Mann *et al.*, 2015). Polymer ionization causes bond cleavage (scission) (Malek and Chong, 2002; Yamauchi *et al.*, 2003; El-Saftawy *et al.*, 2016), cross-linking, degradation, emission of atoms and molecules, creation of the free radicals and formation of saturated and unsaturated groups with stimulated evolution of gases and new functional groups (El-Saftawy *et al.*, 2014; Hassan *et al.*, 2015). The processes of formation of organic compounds in irradiated material are associated with the chain scissoring, re-polymerization, cross linking and atomic displacements (Elmaghraby, 2017), which result in Synthesis of different substances (Badawy *et al.*, 2018). Water-free molecules, carbon oxides and alcoholic compounds with OH – group are the main products of these processes (Yamauchi *et al.*, 2003; Mori *et al.*, 2013). Thus, such radiation induced damage and the oxidative degradation can cause chemical changes in the polymer structure with an accumulation of various new functional groups as carbonyls (C=O), carboxyls (-COOH) and hydroxyls (O-H) (Clough and Shalaby, 1996; Rivaton and Arnold, 2008; Elmaghraby and Talat, 2010; Sahoo *et al.*, 2014).

The present work is devoted to understand the difference between gamma ray effects and neutron influence on organic materials in order to interpret the change occurred in organic matter that coexists with nuclear tests. Our motivation aimed to inspect and compare the potential changes in the chemical properties of CR-39 detector induced by neutron and gamma irradiation and to discover the actual physicochemical alterations occurred. These chemical changes of PADC polymer detectors (CR-39) resulting from irradiation can be readily characterized by spectroscopic techniques such as Fourier transform infrared (FTIR) which could be confirmed by statistical correlations. Peak absorbance at various wave numbers was correlated with doses applied as well as with each other at definite wave number. Moreover, we investigated dose-dependent changes in chemical properties of the detectors aiming at improving an alternative method to estimate neutron doses.

## EXPERIMENTAL METHODS

### Sampling

The material under investigation was PADC nuclear track detector TASTRAK type (manufactured by Track Analysis System Ltd., UK) with thickness 1 mm and density  $1.32 \text{ g/cm}^3$ . It is commercially available as CR-39 with chemical composition of  $[\text{C}_{12}\text{H}_{18}\text{O}_7]_n$  and mass composition (40.8% oxygen ( $M= 15.9994$ ), 52.5% carbon ( $M= 12.0107$ ), 6.6% hydrogen ( $M= 1.0079$ ) which is close to the contents of human tissue (Zhou *et al.*, 2007; Sahoo *et al.*, 2015). Its chemical structure is indicated in Fig. 1. The samples were accurately cut from the same sheet in  $1 \times 1 \text{ cm}^2$  dimensions (to guarantee the same manufacturing conditions and homogeneity between the samples) and cleaned with ethanol to remove any stuck dust. PADC samples were then prepared for irradiation.

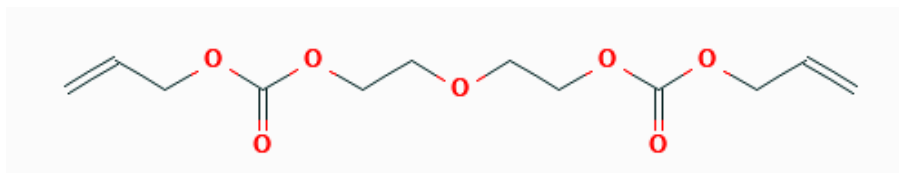


Fig. 1: Monomer Structure of PolyAllyl Diglycol Carbonate (CR-39) polymer.

### Irradiation facilities

Gamma irradiation was carried out using a standard gamma cell employing  $^{60}\text{Co}$  in nuclear research center, Egyptian atomic energy authority.

This gamma cell is qualified to expose the sample with  $2.1 \text{ kGy/h}$  at the time of irradiation. A series of samples were irradiated with doses from  $(5 \pm 1) \times 10^3 \text{ Gy}$  to  $(3.0 \pm 0.6) \times 10^6 \text{ Gy}$ .

Neutron irradiation was done using fast channel in ETRR-2 research reactor using pneumatic arm position 2 for sample delivery (Shaat, 2010). The samples were irradiated for different time periods ranging from 0.67 h to 4 h with average thermal flux of about  $\sim (3 \pm 1) \times 10^{11} \text{ cm}^{-2}\text{s}^{-1}$  and corresponding average integrated neutron flux of about  $(1.424 \pm 0.03) \times 10^{13} \text{ cm}^{-2}\text{s}^{-1}$  (Elmaghraby *et al.*, 2020). We chose the time range of neutron irradiation for the PADC samples due to the following reasons: the insensitivity of PADC materials at low dose in which the minimum time required to observe the visual change of sample appearance was 0.67 h (Talat and Elmaghraby, 2010). While, for irradiation time periods longer than 4h, the sample is completely damaged. The neutron doses were specified by the irradiation time and the fluence to

dose conversion factor value of about  $(3.034 \pm 0.06) \times 10^{-11} \text{ Gy cm}^2$  (Elmaghraby *et al.*, 2020). The applied neutron and gamma irradiation details are indicated in Table 1.

Table 1: Dose values for neutron and gamma irradiated PADC samples. Sample labeled P refers to pristine PADC detector while sample labels that begin with N and G refer to neutron irradiated and gamma irradiated PADC detectors, respectively.

Sample code	Irradiation time (h)	Neutron dose equivalent ( $\times 10^6 \text{ Gy}$ )
P	0	0
N1	0.67	$(1.07 \pm 0.1)$
N2	1	$(1.7 \pm 0.1)$
N3	1.5	$(3.9 \pm 0.2)$
N4	3	$(5.01 \pm 0.7)$
N5	4	$(6.2 \pm 0.9)$
		<b>Gamma-ray dose (<math>\times 10^6 \text{ Gy}</math>)</b>
G1	2.45	$(5 \pm 1) \times 10^{-3}$
G2	24.55	$(5 \pm 1) \times 10^{-2}$
G3	98.2	$(2 \pm 0.4) \times 10^{-1}$
G4	245	$(5 \pm 1) \times 10^{-1}$
G5	490	$(1.0 \pm 0.2)$
G6	981	$(2.0 \pm 0.4)$
G7	1472	$(3.0 \pm 0.6)$

### Measurement techniques

For neutron flux measurements, neutron activation monitors of iron oxide have been employed. Iron oxide has been used instead of metallic iron to avoid oxidative corrosion at monitor surface which may affect the results. The iron oxide monitors were synthesized in pure form using microwave-assisted synthesis and provided by Aldrich chem. Co. Ltd of 99.99% purity (Abd El Aal *et al.*, 2019; Elmaghraby *et al.*, 2020). The neutron monitoring reactions was determined through the decay lines of  $^{54}\text{Mn}$  ( $T_{1/2}=312.2 \text{ d}$ ,  $E=834.848 \text{ keV}$ , 100%) (Dong and Junde, 2014) and  $^{59}\text{Fe}$  ( $T_{1/2}=44.495 \text{ d}$ ,  $E=1291.59 \text{ keV}$ , 43.2%) (Baglin, 2002; Basunia, 2018; Elmaghraby *et al.*, 2020).

All gamma ray measurements were carried out by ORTEC HPGe detector. The efficiency calibration was done using standard sources with uncertainty less than 7%. The efficiency of the germanium detector was calibrated using decay from standard sources of  $^{60}\text{Co}$  (Browne and Tuli, 2013),  $^{133}\text{Ba}$  (Khazov, 2011),  $^{137}\text{Cs}$  (Browne and Tuli, 2007) and  $^{152,154}\text{Eu}$  (Martin, 2013; El-Said *et al.*, 2018).

### Characterization

The physicochemical induced effects of gamma and neutron irradiation in CR-39 PADC detectors have been characterized by FTIR spectrometry using FTIR spectrometer type, VERTEX-70, from Germany. This instrument recorded the spectra in the wavenumbers range of  $400\text{--}4000 \text{ cm}^{-1}$  with a resolution of  $4 \text{ cm}^{-1}$ . The pristine and irradiated samples were investigated, non-destructively, by infrared spectroscopy (i.e. without mixing them with KBr, as usual in FTIR). This technique was used mainly to study the dose-dependent changes in the absorbance due to different vibration modes of the functional groups in the molecules. Furthermore, for comparing between gamma-ray and neutrons irradiation effects.

### Statistical analysis

In FTIR spectra, the analysis of the main absorption bands validate the investigation of various changes occurred in PADC polymers. Comparison between results of absorption band integration with the other selected bands, simplifies the determination of the extinction coefficients and improves the quantitative feature of

FTIR (Patrick landais, 1995). Moreover, verifying FTIR spectral information with that obtained by other spectroscopic techniques.

## RESULTS AND DISCUSSION

### *Gamma dose calculations*

The neutron-irradiated samples were exposed to gamma irradiation during the time of irradiation and after removal from the neutron field until dispatching the container. This was due to the existence of  $^{54}\text{Mn}$ ,  $^{59}\text{Fe}$ , and the  $^{60}\text{Co}$  (Elmaghraby *et al.*, 2020). This gamma dose was measured using  $\gamma$ -dosimeter at the surface of the aluminum container at which the sample was placed on its axial center. Dose was estimated at the sample position using inverse-square law with uncertainty of 25%. This  $\gamma$ -dose was measured frequently during contact period while, the estimated variation of this dose versus time is depicted from the decay scheme of  $^{54}\text{Mn}$ ,  $^{59}\text{Fe}$ , and  $^{60}\text{Co}$  nuclei (Elmaghraby *et al.*, 2020). Integration throughout the contact time between the PADC samples and the iron monitors yields the accumulated  $\gamma$ -dose which was found to be  $0.4\pm 0.1$  Gy for all samples (Elmaghraby *et al.*, 2020).

### *Fourier transform infrared (FTIR) spectroscopic studies*

As mentioned in sec 1.1, the impact of radiation on organic material may be varied according to various radiation types. The basic effect of neutron is atomic displacement (due to atoms recoil) (Elmaghraby, 2017) and neutron capture (Firestone and Revay, 2016) while the main effect of gamma radiation is bond breakage (Elmaghraby and Seddik, 2015). These effects lead to formation of active radicals of  $\text{H}^+$ ,  $\text{OH}^-$ , and  $\text{H}_2\text{O}-2$  as well as molecules such as  $\text{H}_2\text{O}$ ,  $\text{CO}$ , and  $\text{CO}_2$  (Zaki *et al.*, 2016).

Hence, the alterations in vibrational levels of the irradiated PADC samples can be observed in Fourier transform infrared (FTIR) spectra. FTIR spectra of pristine and irradiated polymer samples were carried out in mid-infrared spectrum region ( $400-4000\text{ cm}^{-1}$ ) and was shown in Fig.2 which is an infrared absorption spectra model of PADC samples, explicitly, pristine sample with linear absorption coefficient  $\alpha_{\text{sample}}$  specified from the relation

$$\alpha_{\text{sample}} = \frac{1}{t_{\text{sample}}} \ln \frac{100}{T_{\text{IR}}\%} [\text{cm}^{-1}],$$

Where,  $t_{\text{sample}}$  is the sample thickness in cm, and  $T_{\text{IR}}\%$  is the percentile infrared transmittance at the specific wavenumber  $k$ . Fig.2 and Table 2 represents the most important characteristic absorption peaks. The relative modifications in the intensities of the corresponding bands can be estimated from the relative functional groups present in the PADC polymer.

The whole analysis of FTIR spectra of gamma irradiated samples showed an increase in absorbance with gamma dose by distinguished bands of the above mentioned function groups for irradiated samples compared to pristine one, this illustrated in (Fig. 3 & Table 2).

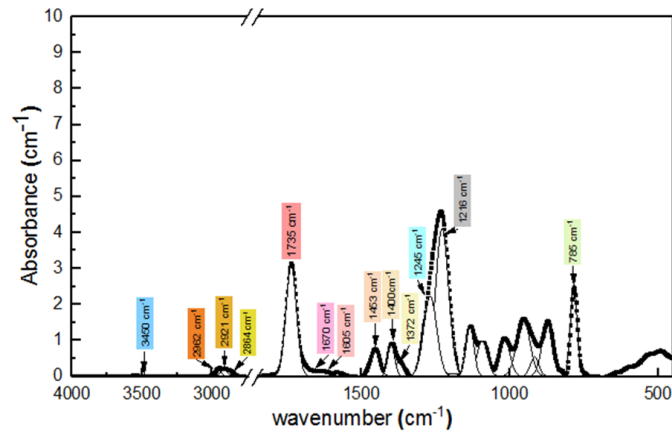


Fig. 2: Spectra of Infrared absorption for pristine sample (labels details are discussed in table 2)

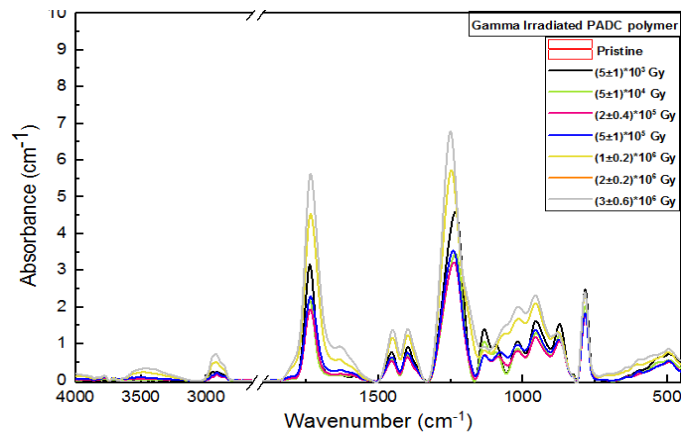


Fig.3: FTIR absorption spectra for pristine and gamma irradiated PADC polymer

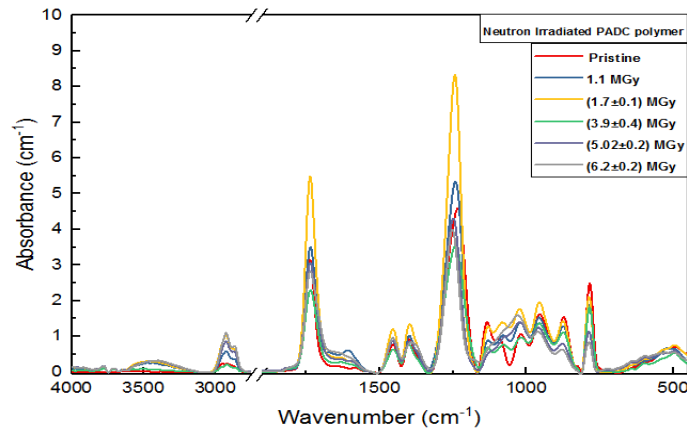


Fig. 4: FTIR absorption spectra of pristine and neutron irradiated PADC polymer.

In case of neutron irradiation, there is an oscillating behavior occurred which showed an increase in absorbance with increasing absorbed dose in some bands while a decrease in absorbance for another bands, see (Fig.4 & Table 2). Such increase or decrease in absorbance with dose may be assigned to the formation of free radicals, cross-linking and degradation of polymeric chains due to irradiation (Srivastava *et al.*, 2002; Kumar and Singh, 2013; El-Saftawy *et al.*, 2016).

Table 2: Characteristics of the prominent peaks in the FTIR spectra of pristine, neutron and gamma irradiated PADC polymers.

Peak position (cm <sup>-1</sup> )	Functional group modes	Absorbance (cm <sup>-1</sup> )													
		pristine	Neutron dose (*10 <sup>6</sup> Gy)						Gamma dose (Gy)						
			1.07±01	1.7±0.1	3.9±0.2	5.01±0.7	6.2±0.9	(5±1)×10 <sup>3</sup>	(5±1)×10 <sup>4</sup>	(2±0.4)×10 <sup>5</sup>	(5±1)×10 <sup>5</sup>	(1.0±0.2)×10 <sup>6</sup>	(2.0±0.4)×10 <sup>6</sup>	(3.0±0.6)×10 <sup>6</sup>	
3450	-OH stretching	0.01211	0.25157	0.3017	0.07653	0.30617	0.31674	0.01211	0.02679	0.04922	0.07653	0.22021	0.32545	0.32545	
2962	sp <sup>3</sup> C-H stretching	0.22001	0.38299	0.68068	0.12965	0.53219	0.63913	0.22001	0.13722	0.08942	0.12965	0.40568	0.56375	0.56375	
2921	CH <sub>2</sub> asymmetric stretching	0.23178	0.58444	1.01554	0.21078	0.85207	1.09051	0.23178	0.16283	0.16172	0.21078	0.50508	0.71589	0.71589	
2864	sp <sup>3</sup> C-H stretching	0.15924	0.36452	0.64044	0.12652	0.56909	0.72762	0.15924	0.10908	0.0961	0.12652	0.3032	0.4152	0.4152	
1735	conjugated C=O stretching	3.14686	3.50499	5.48562	2.29178	3.05652	2.82347	3.14686	2.18422	1.93114	2.29178	4.51813	5.61076	5.61076	
1670	Non-conjugated C=O stretching	0.17916	0.55862	0.46696	0.29217	0.43047	0.6087	0.17916	0.14847	0.18723	0.29217	0.66253	1.02708	1.02708	
1605	Conjugated C=C stretching	0.10596	0.61139	0.31526	0.23391	0.31744	0.42586	0.10596	0.1287	0.15661	0.23391	0.42714	0.70599	0.70599	
1453	C-H bending of CH <sub>2</sub>	0.76563	0.86625	1.20072	0.63682	0.86622	0.95351	0.76563	0.57548	0.52318	0.63682	1.16274	1.37625	1.37625	
1400	CH <sub>3</sub> symmetric	0.90851	1.01233	1.31884	0.76029	0.84244	0.77982	0.90851	0.68211	0.63916	0.76029	1.23036	1.39332	1.39332	
1372	C-H bending for CH <sub>3</sub>	0.45312	0.52221	0.75184	0.3684	0.57831	0.72567	0.45312	0.34489	0.30246	0.3684	0.63008	0.75239	0.75239	
1245	C-O-C stretching vibrations	4.27492	5.26259	8.27274	3.49466	4.28087	3.84775	4.27492	3.23141	3.13279	3.49466	5.7237	6.67201	6.67201	
1216	C-O-C stretching vibrations	3.74271	3.06419	3.62571	2.43907	1.67566	1.26313	3.74271	2.81751	2.35944	2.43907	3.39058	3.54565	3.54565	
785	C-H out-of-plane bending	2.48045	1.88123	2.0926	1.82285	1.12347	0.82066	2.48045	2.02057	1.75495	1.82285	2.36789	2.40088	2.40088	

### Interpretation of FTIR spectra for neutron and gamma irradiated PADC samples

The variations in absorption with gamma dose and neutron absorbed dose have been interpreted in terms of chemical changes as emphasized from infrared spectra (Figs. 3 & 4), and the following observations were obtained:

A broad absorption peak at  $3450\text{ cm}^{-1}$  which attributed to  $\text{-OH}$  stretching vibrational band was observed to have an increase in absorbance with dose for gamma irradiated samples. This increase in hydroxyl ( $\text{-OH}$ ) group may be due to the scission occurred in the  $\text{-CH}_2\text{-O-CH}_2\text{-}$ , which lead to the formation of the  $\text{-OH}$  group. While the dose increases, the band becomes gradually broader. This indicates that a degradation process prevails at higher doses. Also, this degradation caused ordering in the irradiated samples to some degree, thus formation of hydroxyl group leads to water formation (Nouh *et al.*, 2009; Sahoo *et al.*, 2014; El-Saftawy *et al.*, 2016). Similar is the case of neutron irradiation, but there is more modification as compared to gamma irradiation for the corresponding band. Thus, both neutron and gamma irradiation caused reordering in the irradiated samples.

Absorbance of the summed-peaks at positions  $1216\text{ cm}^{-1}$  and  $1245\text{ cm}^{-1}$  increases upon gamma irradiation. In contrast, the measurements showed a decrease in absorbance for neutron irradiated samples. This indicates that scission occurred at the carbonate site with probable elimination of carbon dioxide ( $\text{CO}_2$ ) or carbon monoxide ( $\text{CO}$ ) (Elmaghraby and Seddik, 2015).

A similar behavior was observed for the absorbance at  $1735\text{ cm}^{-1}$  (corresponding to  $\text{C=O}$  conjugated stretching group) which showed the same way for the absorbance of  $\text{C=O}$  with for both gamma and neutron irradiated samples (Nouh *et al.*, 2009).

Furthermore, the absorbance in the characteristic bands at positions  $2864\text{ cm}^{-1}$ ,  $2921\text{ cm}^{-1}$ , and  $2962\text{ cm}^{-1}$  which corresponding to the  $\text{sp}^3\text{ C-H}$  stretching vibrations, increases with dose for gamma and neutron irradiated samples. These result indicate the existstness of a bond breakage nevertheless, at one of the carbon positions in the molecule backbone.

The  $1372\text{ cm}^{-1}$  peak which related to the  $\text{C-H}$  bending vibration of  $\text{CH}_3$  group follows the same behavior of  $\text{sp}^3\text{ C-H}$  stretching vibrations bands. The peak absorbance was observed to be increased with ( $\gamma$  or  $n$ ) irradiation (except for gamma ray doses under the  $(2\pm 0.04) \times 10^5\text{ Gy}$ , and this could be due to the scission of polymer chain at the beginning of irradiation and crosslinking at high doses (El-Saftawy *et al.*, 2016). Thus, such results explained that many extra bonded hydrogen appeared due to either  $\gamma$  or  $n$  irradiation doses.

Moreover, the sum-peak appeared at  $1605\text{ cm}^{-1}$  and  $1670\text{ cm}^{-1}$  which assigned for the conjugated and non-conjugated  $\text{C=C}$  stretching vibrations have a comparable behavior for  $\gamma$ -irradiated samples and  $n$ -irradiated samples. The peak absorbance undergoes an increase with increasing gamma doses and this could be attributed to the growing number of double bonded carbon. However, the absorbance was observed to be decreased upon neutron irradiation, which could be attributed to the dissociation of  $\text{C=C}$  bond at high neutron doses (Sahoo *et al.*, 2014).

The variation of absorbance at  $1400\text{ cm}^{-1}$  appeared to be likely increased with increasing gamma irradiation dose. On other side, the absorbance decreased with the increase of neutron dose. Such decrease in absorbance could lead to destruction of polymer due to neutron irradiation. The same trend is assigned to the adjacent bending absorption peak at  $1453\text{ cm}^{-1}$ . The absorbance at  $785\text{ cm}^{-1}$  (corresponding to the  $\text{C-H}$  out-of-plane deformation vibrations), behaves similar to the  $\text{CH}_2$  bending

vibration with no variation between gamma ray response and neutron response of the material.

Effects of gamma and neutron irradiation on the studied PADC have a correspondence behavior at low doses. While the PADC samples get more altered with increasing dose. On other side, the difference is accompanied to energy deposition of radiation in the material which is a time dependent process.

For gamma irradiation,  $\gamma$ -energy is transferred to the electrons in the system; where the secondary electrons are responsible for the subsequent radiation effect as they retarded within the material. This effect may cause the bond breakage for weak bonds such as C-H, C-O, and C-C with different possibilities.

On the other hand, neutron energy deposition behaves in different manner. Largely, it is represented in H-atom displacement via neutrons scattering by atoms in the material which transfer amount of its energy to the constituents of the material (Elmaghraby, 2017). Atomic displacement depends on neutron energy and has very small probability at thermal neutrons where the recoil nucleus does not have sufficient energy to break a chemical bond. While, atomic displacement is more probable for hydrogen due to its weak bond and light weight. By recoil of hydrogen atom, it induces the chemical reaction that alter the C-O-C, C=O, C=C or forming the -OH radical.

#### ***Statistical correlations***

Correlation is the statistical summary of the relationship between variables. Thus, it is important to discover and quantify the degree to which variables in the dataset are dependent upon each other.

If a correlation is positive with coefficient +1, it is called a perfect direct linear relationship meaning that both variables move in the same direction. While negative correlation with coefficient -1 means that when one variable's value increases, the other variables' values decrease. This called a perfect inverse linear relationship. Some values in the open interval (-1, 1) in all other cases, indicating the degree of linear dependence between the variables. Correlation can also be zero, which indicates that variables are not correlated.

In this research study, the prominent infrared bands indicated in table 2 have been integrated in order to draw correlations between band intensities for neutron and gamma irradiated samples. The correlations derived from FTIR analysis of the studied samples were used to deduce the relation between changes occurred in the selected FTIR bands due to irradiation. Data derived from the integration of major infrared bands have already been correlated with each other and the following results were obtained. Such data took into account the possible variations of the absorptivity of each infrared band as a function of the modifications in the organic matter structure (Patrick landais, 1995).

In (Fig.5), a strong direct linear correlation between the two integrated absorption was observed due to gamma irradiation. It can be deduced that the formation of water is directly proportional to the absorption of CH<sub>3</sub> symmetric group. In contrast for neutron irradiation, there was weak inverse correlation between the absorption of the two bands. This indicates that formation of -OH radical could be due to the dissociation of CH<sub>3</sub> bonding. Such action could be explained by the decrease in the integrated absorption of the CH<sub>3</sub> group.

The same behavior of corelations in (Fig. 5) was noticed in (Fig.6). The integrated absorption at 1453 cm<sup>-1</sup> showed the same correlation for the C-H bending of CH<sub>2</sub> integrated absorption with -OH integrated absorption for both gamma and neutron irradiated samples.

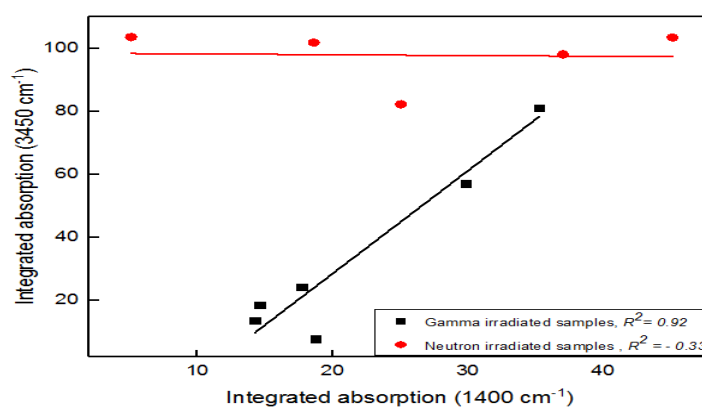


Fig. 5: Integrated absorption of CH<sub>3</sub> symmetric at 1400 cm<sup>-1</sup> and formation of (-OH) hydroxyle group at 3450 cm<sup>-1</sup>, with linear trendline and R<sup>2</sup> value .

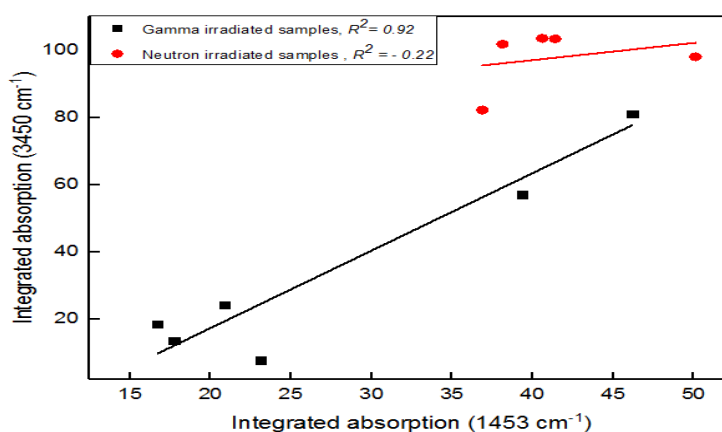


Fig.6: Integrated absorption of C-H bending of CH<sub>2</sub> at 1453 cm<sup>-1</sup> and formation of (-OH) hydroxyle group 3450 cm<sup>-1</sup> with linear trendline and R<sup>2</sup> value' .

For gamma irradiation (Fig. 7), a correlation between the integrated absorption of the Conjugated C=C stretching at 1606 cm<sup>-1</sup> and formation of (-OH) hydroxyle group at 3450 cm<sup>-1</sup> was observed to be almost perfect direct linear relation with an excellent value of R<sup>2</sup> . For neutron irradiated samples, a weak linear correlation between the two integrated bands was observed. This indicates that the integrated absorption of the two bands increase with radiation dose either gamma or neutron irradiation. Such increase were observed to be stronger for gamma irradiation in comparison to neutron irradiation.

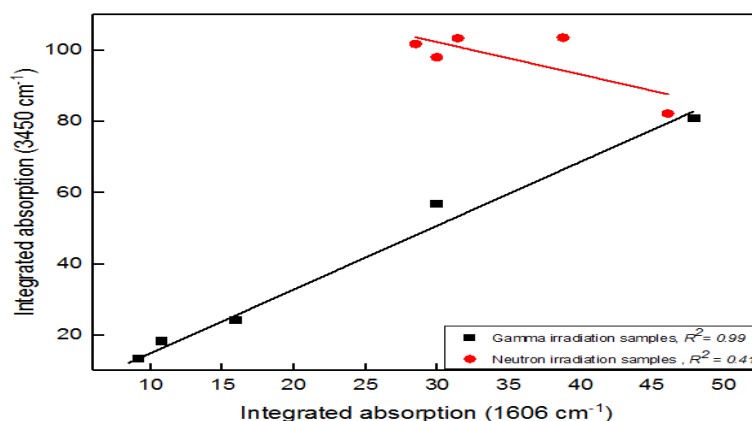


Fig. 7: Integrated absorption of Conjugated C=C stretching at 1606 cm<sup>-1</sup> and formation of (-OH) hydroxyle group at 3450 cm<sup>-1</sup>, with linear trendline and R<sup>2</sup> value.

In (Fig. 8), The Integrated absorption of conjugated C=O stretching at  $1735\text{ cm}^{-1}$  showed a very good direct linear correlation with formation of (–OH) hydroxyle at  $3450\text{ cm}^{-1}$  due to gamma irradiation. While a very weak inverse linear correlation was observed due to neutron irradiation. This could be indicates the inverse trend of gamma and neutron irradiation effects on the studied samples.

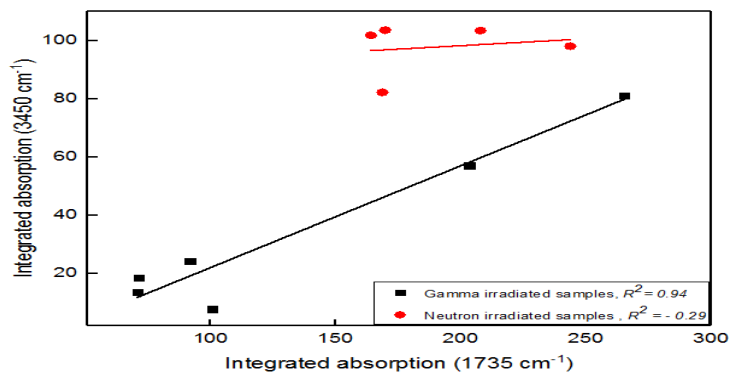


Fig. 8: Integrated absorption of conjugated C=O stretching at  $1735\text{ cm}^{-1}$  and formation of (–OH) hydroxyle at  $3450\text{ cm}^{-1}$ , with linear trendline and  $R^2$  value.

For the correlations in (Figs. 9 & 10), nearly the same effect was observed for gamma and neutron irradiation. Such explanation because the integrated absorption of  $\text{sp}^3$  C-H stretching at  $2864\text{ cm}^{-1}$  as well as the integrated absorption of  $\text{CH}_2$  asymmetric stretching at  $2921\text{ cm}^{-1}$  and formation of (–OH) hydroxyle group at  $3450\text{ cm}^{-1}$  showed a very good strong direct correlation. The increase or decrease in absorbance for these two bands almost have the same trend for both gamma and neutron applied doses.

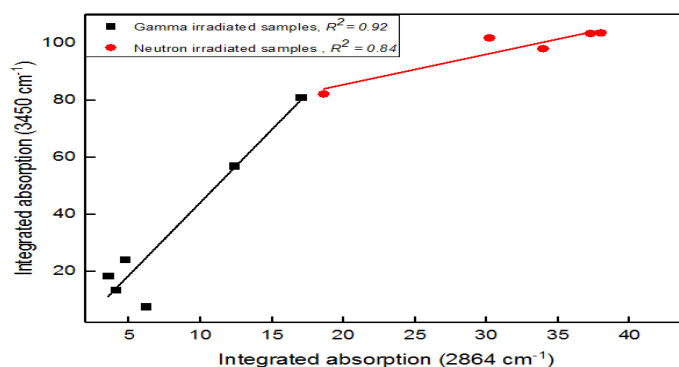


Fig. 9: Integrated absorption of  $\text{sp}^3$  C-H stretching at  $2864\text{ cm}^{-1}$  and formation of (–OH) hydroxyle group at  $3450\text{ cm}^{-1}$ , with linear trendline and  $R^2$  value.

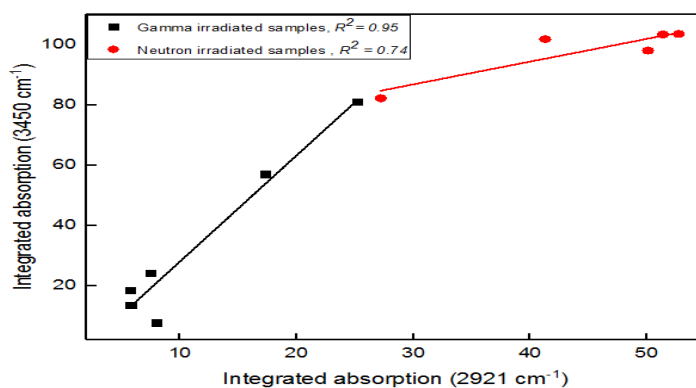


Fig.10: Integrated absorption of  $\text{CH}_2$  asymmetric stretching at  $2921\text{ cm}^{-1}$  and formation of (–OH) hydroxyle group at  $3450\text{ cm}^{-1}$ , with linear trendline and  $R^2$  value

In (Fig. 11), the integrated absorption of  $sp^3$  C-H stretching at  $2962\text{ cm}^{-1}$  is good correlated to the formation of (-OH) hydroxyle group at  $3450\text{ cm}^{-1}$  with direct correlation for gamma irradiated samples. On the other hand for neutron irradiated samples, the two bands was observed to be medium direct correlation.

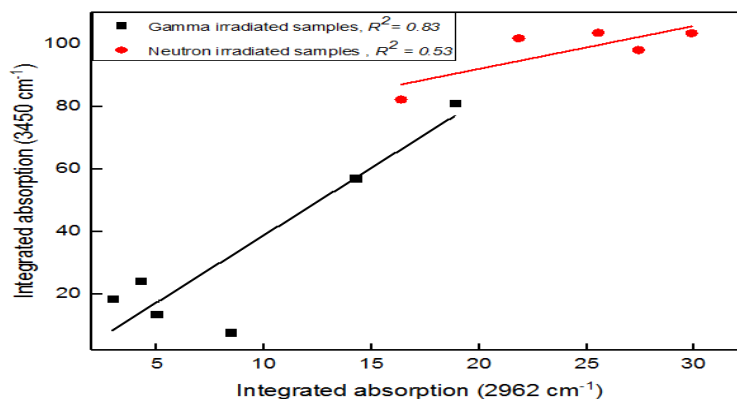


Fig.11: Integrated absorption of  $sp^3$  C-H stretching at  $2962\text{ cm}^{-1}$  and formation of (-OH) hydroxyle group at  $3450\text{ cm}^{-1}$ , with linear trendline and  $R^2$  value.

## CONCLUSION

On the basis of the obtained results, CR-39 PADC polymer was demonstrated to have neutron dosimetric property appropriate for estimation of high neutron fluencies. In addition, the results prove the living effect of radiation on the polymeric material. These findings are confirmed by FTIR measurements in which, gamma and neutron irradiation alters the infrared absorption and the intensity of the C=O, C=C and C-O-C vibrations. The correspondence and difference between gamma ray and neutron irradiation impact confirmed at least two different mechanisms for gamma and neutron interaction with matter. Degradation occurred as a result of gamma irradiation, after which some functional groups undergo crosslinking. Such effect may be due to the increase in the number of conjugated chains. While, Neutron irradiation resulted in oxidation or displacing hydrogen atoms causing chain break. This was emphasized by modifications of the IR spectra seen in most regions especially, the carbonyl and hydroxyl regions.

More specific description, there is an obvious relationship with a good correlation between the growth of the carbonyl group (C=O) at  $1735\text{ cm}^{-1}$  and the gamma dose due to the oxidation of the polymer. By contrast, carbonyl group (-C=O) degrades under neutron irradiation and the absorbance for such band decreased by increasing neutron dose. Such observation indicates that the carbonyl groups are the most sensitive groups to radiation. The same trend was observed for the summed-peaks at positions  $1216\text{ cm}^{-1}$  and  $1245\text{ cm}^{-1}$  indicating a probable elimination of carbon dioxide ( $\text{CO}_2$ ) or carbon monoxide (CO). Furthermore, the appearance of OH peak around  $3450\text{ cm}^{-1}$  for both gamma and neutron irradiated samples. This is due to the rupture occurred in the  $-\text{CH}_2-\text{O}-\text{CH}_2-$ , forming new radicals and thus OH generation. In addition, the correlations set between some bands and formation of water due to growth of (-OH) hydroxyl group supported the interpretation of the results obtained. Furthermore, such correlations confirmed the correspondence and differences between gamma and neutron irradiation effects.

In conclusion, and throughout the obtained results of, we can provide a vision to the upcoming steps of neutrons and gamma ray interaction with organic materials.

These approaches open the way to radiation treatment and synthesis for materials via the improvement of techniques used, in addition to dosimetric purposes. The suitability for the development of such PADC materials for various applications should be pursued. We also recommend applying other analysis techniques to yield a wealth of information for the early improvements of these materials.

From biological side, the radiation induced changes in organic material composition and production of free radicals could lead to new properties or material damage. So, we deduced that radiation carries a finite risk to human as well as marine environment due to the possible induction diseases or genetic damage in offspring as well as marine organisms, and this risk is directly proportional to the accumulated dose.

Moreover, the results indicated production of water after irradiation and the water itself absorbs radiation. This is a very good shielding material, and a little exposure will be from the water outside the animal. Principally all exposure will be from radioactive materials ingested by the animal. Thus, disposal of radioactive wastes which originates from nuclear tests into the marine environment has hazardous consequences. Such hazards could be presented in terms of the subsequent increase in radiation exposure of human and aquatic populations. So, we recommend a suitable radioactive waste management to save marine life. Also, we suggest further future research on the components of marine environment (water, plants, animals,..etc) to reduce the radioactivity levels and guarantee safe life for marine populations.

## REFERENCES

- Abd El Aal, S.; Abdelhady, A.; Mansour, N.; Hassan, N. M.; Elbaz, F. and Elmaghraby, E. K. (2019). Physical and chemical characteristics of hematite nanoparticles prepared using microwave-assisted synthesis and its application as adsorbent for Cu, Ni, Co, Cd and Pb from aqueous solution. *Materials Chemistry and Physics*, 121771. Doi:10.1016/j.matchemphys.2019.121771.
- Abdul-Kader, A. M.; Zaki, B. M. F.; El-Badry, A. (2014). Modified the optical and electrical properties of CR-39 by gamma ray irradiation. *J. Radiat. Res. Appl. Sci.*, 7(3): 286-291. Doi:10.1016/j.jrras.2014.05.002.
- Badawy, Z. M.; Zaki, M. F. and Elmaghraby, E. K. (2018). Investigations on the Migration of Radiation-Induced Compounds in Polymeric Nuclear Track Detectors. *Arab J. Nucl. Sci. Appl.*, 51 (3): 1-8. Doi:10.21608/ajnsa.2017.1868.1002.
- Baglin, C. M. (2002). Nuclear data sheets for A = 59. *Nucl. Data. Sheets*, 95(2): 215-386. Doi:10.1006/ndsh.2002.0004.
- Basunia, M. S. (2018). Nuclear Data sheets for A=59. *Nucl. Data Sheets*, 151, 1 – 333. Doi:10.1016/j.nds.2018.08.001.
- Bo Liu, Pu-Cheng Wang, Yin-Yong Ao, Yan Zhao, You An, Hong-Bing Chen and Wei Huang (2017). Effects of combined neutron and gamma irradiation upon silicone foam. *Radiat. Phys. Chem.*, 133, 31–36. Doi:10.1016/j.radphyschem.2016.12.005.
- Browne, E and Tuli, J. K. (2007). Nuclear data sheets for A = 137. *Nucl. Data Sheets*, 111(10): 2173 – 2318. Doi:10.1016/j.nds.2007.09.002.
- Browne, E. and Tuli, J., K. (2013). Nuclear data sheets for A = 60. *Nucl. Data. Sheets*, 114(12): 1849 – 2022. Doi:10.1016/j.nds.2013.11.002.
- Castillo, F.; Espinosa, G.; Golzarri, J. I.; Osorio, D.; Rangel, J.; Reyes, P.G. and Herrera, J.J.E. (2013). Fast neutron dosimetry using CR-39 track detectors with

- polyethylene as radiator. *Radiat. Meas.*, 50: 71-73. Doi: 10.1016/j.radmeas.2012.09.007.
- Claudia, R.; Benitez-Nelson; Sabine Charmasson; Ken Buesseler; Minhan Dai; Michio Aoyama; Nria Casacuberta; Jos Marcus Godoy; Andy Johnson; Vladimir Maderich; Pere Masqu; Marc Metian; Willard Moore; Paul, J.; Morris and John, N. Smith (2018). Radioactivity in the Marine Environment: Understanding the Basics of Radioecology. *Limnology and Oceanography e-Lectures*, 8: 170– 228. Doi:10.1002/loe2.10007.
- Clough, R. L. and Shalaby S. W. (1996). Irradiation of Polymers: Fundamentals and technological applications. American Chemical Society., Washington, DC.
- Dong, Y. and Junde, H. (2014). Nuclear data sheets for A = 54. *Nucl. Data. Sheets*, 121: 1 – 142. Doi:10.1016/j.nds.2014.09.001.
- El-Badry, B. A.; Zaki, M. F.; Abdul-Kader, A. M.; Tarek, M.; Hegazy, A.; Morsy, A. (2009). Ion bombardment of Poly-Allyl-Diglycol-Carbonate (CR-39). *Vacuum*, 83: 1138–1142. Doi:10.1016/j.vacuum.2009.02.010.
- Elmaghraby, E. K. and Seddik, U. (2015). Thermophysical properties and reaction kinetics of irradiated poly allyl diglycol carbonates nuclear track detector. *Radiat. Eff. Defects. Solids*, 170, 621–629. Doi:10.1080/10420150.2015.107733.
- Elmaghraby, E. K.; Saad Abdelaal; Abdelhady, A. M.; Samar Fares, Salama, S. and Mansour, N.A. (2020). Experimental determination of the fission-neutron fluence-to-dose conversion factor. *Nuclear Inst. and Methods in Physics Research, A.*, 949, 162889. Doi: 10.1016/j.nima.2019.162889.
- Elmaghraby, E. K. (2017). Resonant neutron-induced atomic displacements. *Nucl. Instrum. Methods Phys. Res. B*, 398, 42 – 47. Doi:10.1016/j.nimb.2017.03.054.
- Elmaghraby, E. K. and Talat, S. A. (2010). Investigation of the fluorescence emitted from polyallyl diglycol carbonate modified by gamma-ray radiation excited by UV radiation. *Radiat. Eff. Def. Solids.*, 165, 4, 321–328. Doi: 10.1080/10420150903452252.
- El-Saftawy, A. A.; Abdel Reheem, A. M.; Kandil, S. A.; Abd El Aal, S. A. and Salama, S. (2016). Comparative studies on PADC polymeric detector treated by gamma radiation and Ar ion beam. *Applied Surface Science*, 371: 596-606. Doi:10.1016/j.apsusc.2016.03.044.
- El-Saftawy, A. A.; Elfalaky, A.; Ragheb, M. S. and Zakhary, S. G. (2014). Electron beam induced surface modifications of PET film. *Radiat. Phys. Chem.*, 102: 96-102. Doi:10.1016/j.radphyschem.2014.04.025.
- El-Saftawy, A. A.; Abd El Aal, S. A.; Hassan, N. M. and Abdelrahman, M. M. (2016). Optical and chemical behaviors of CR-39 and Makrofol plastics under low-energy electron beam irradiation. *Japanese Journal of Applied Physics*, 55, 076401. Doi: 10.7567/jjap.55.076401.
- El-Said, H.; Ramadan, H. E.; Elmaghraby, E. K. and Amin, M. (2018). Development of granular radioactive reference source from <sup>152,154</sup>Eu adsorbed on tin tungstate matrix. *Radiochimica Acta*, 106, 8. [Doi: 10.1515/ract-2017-2885](https://doi.org/10.1515/ract-2017-2885).
- Firestone, R. B. and Revay, Z. (2016). Thermal neutron capture cross sections for <sup>16,17,18</sup>O and <sup>2</sup>H. *Phys. Rev. C.*, 93, 044311. Doi:10.1103/PhysRevC.93.044311.
- Hassan, A.; El-Saftawy, A. A.; Abd El Aal, S. A. and El Ghazaly, M. (2015). Irradiation influence on Mylar and Makrofol induced by argon ions in a plasma immersion ion implantation system. *Appl. Surf. Sci.*, 347: 784-792. Doi: 10.1016/j.apsusc.2015.04.179.
- Khazov, Y.; Rodionov, A. and Kondev, F. (2011). Nuclear data sheets for A = 133. *Nucl. Data Sheets*, 112(4): 855 – 1113. Doi:10.1016/j.nds.2011.03.001.

- Kulwinder Singh Mann; Asha Rani and Manmohan Singh Heer (2015). Shielding behaviors of some polymer and plastic material for gamma-rays, *Radiat. Phys. Chem.*, 106, 247–254. Doi: 10.1016/j.radphyschem.2014.08.005.
- Kumar, R. and Singh, P. (2013). UV–visible and infrared spectroscopic studies of Li<sup>3+</sup> and C<sup>5+</sup> irradiated PADC polymer. *Results in Physics*, 3: 122-128. Doi:10.1016/j.rinp.2013.07.001.
- Malek, M. A. and Chong, C. S. (2002). Generation of CO<sub>2</sub> in  $\gamma$ -ray irradiated CR-39 plastic, *Radiat. Meas.*, 35: 109-112. Doi: 10.1016/s1350-4487(01)00275-x.
- Martin, M., J. (2013). Nuclear data sheets for A = 152. *Nucl. Data. Sheets*, 114(11): 1497-1847. Doi:10.1016/j.nds.2013.11.001.
- Mee, L. D. and Readman, J. W. (1993). "Nuclear and isotopic techniques for investigating marine pollution." *IAEA Bulletin* 35 (2): 2-8.
- Mori, Y.; Yamauchi, T.; Kanasaki, M.; Hattori, A.; Oda, K.; Kodaira, S.; Konishi, T.; Yasuda, N.; Tojo, S.; Honda, Y. and Barillon, R. (2013). Vacuum effects on the radiation chemical yields in PADC films exposed to gamma rays and heavy ions. *Radiat. Meas.*, 50: 97 – 102. Doi:[10.1016/j.radmeas.2012.07.013](https://doi.org/10.1016/j.radmeas.2012.07.013)
- Nouh, S.A.; Amer, H. and Remon, S.W. (2009). Effect of neutron dose on the structural properties of Makrofol polycarbonate. *Nuclear Instruments and Methods in Physics Research*, 267: 1129–1134. Doi:10.1016/j.nimb.2009.02.049.
- Patrick landais (1995). Statistical determination of geochemical parameters of coal and kerogen macerals from transmission micro-infrared spectroscopy data. *Org. Geochem.*, 23 711-720. Doi: 10.1016/0146-6380(95)00070-U.
- Právǎlie, R. (2014). Nuclear Weapons Tests and Environmental Consequences: A Global Perspective *AMBIO*, 43, 729. Doi: 10.1007/s13280-014-0491-1.
- Rivaton, A. and Arnold, J. (2008). Structural modifications of polymers under the impact of fast neutrons. *Polymer Degradation and Stability*, 93(10): 1864-1868. Doi:10.1016/j.polymdegradstab.2008.07.015.
- Saad, A. F.; Hamed, N. A.; Abdalla, Y. K. and Tawati, D. M. (2012). Modifications of the registration properties of charged particles in a CR-39 polymeric track detector induced by thermal annealing. *Nuclear Instruments and Methods in Physics Research B*, 287, 60–67. Doi:10.1016/j.nimb.2012.07.005.
- Saad, A.F.; Mona, H.; Ibraheim, A.; Nwara, M. and Kandil, S.A. (2018). Modifications in the optical and thermal properties of a CR-39 polymeric detector induced by high doses of  $\gamma$ -radiation. *J.Radiat. Phys. Chem*, 145: 122–129. Doi:10.1016/j.radphyschem.2017.10.011.
- Sahoo, G.S.; Paul, S.; Tripathy, S. P.; Sharma, S. C.; Jena, S.; Rout, S.; Joshi, D.S. and Bandyopadhyay, T. (2014). Effects of neutron irradiation on optical and chemical properties of CR-39: Potential application in neutron dosimetry. *J. Appl. Radiat. Isot.*, 94: 200-205. Doi:10.1016/j.apradiso.2014.08.012.
- Sahoo, G.S.; Tripathy, S. P.; Paul, S.; Sharma, S. C.; Joshi, D. S.; Gupta, A. K. and Bandyopadhyay, T. (2015). Effects of high neutron doses and duration of the chemical etching on the optical properties of CR-39. *J. Appl. Radiat. Isot.*, 101: 114-121. Doi:10.1016/j.apradiso.2015.04.002.
- Sangeeta Prasher; Mukesh Kumar and Surinder Singh (2015). The influence of neutron irradiation in CR-39 polymer. *Oriental Journal of Chemistry*, 31(2): 1201-1204. Doi:10.13005/ojc/310277.
- Shaat, M. (2010). Utilization of ETRR-2 and collaboration. Report IAEA-TM-38728, IAEA, Austeria.
- Siddhartha, Suveda Arya; Kapil Dev; Mohd Shakir; Bashir Ahmed and Wahab, M. A. (2012). Effect of cobalt-60  $\gamma$  radiation on the physical and chemical

- properties of poly (ethylene terephthalate) polymer. *J. Appl. Polym. Sci.*, 125: 3575–3581. Doi:10.1002/app.36397.
- Srivastava, A.; Singh, T. V.; Mule, S.; Rajan, C. R. and Ponrathnam, S. (2002). Study of chemical, optical and thermal modifications induced by 100 MeV silicon ions in a polycarbonate film. *Nucl. Instrum. Methods. Phys. Res. Sect B.*, 192: 402–6. Doi: 10.1016/S0168-583X(02)00493-7.
- Talat, A. S. and Elmaghraby, E. K. (2010). High gamma-ray dose measurement using nuclear track detector. *J. Radiat. Protect. Dosim.*, 140 (3): 218–222. Doi: 10.1080/10420150903452252.
- Yamauchi, T.; Nakai, H.; Somaki, Y. and Oda, K. (2003). Formation of CO<sub>2</sub> gas and OH groups in CR-39 plastics due to gamma-ray and ions irradiation, *Radiat. Meas.* 36: 99-103. Doi: 10.1016/s1350-4487(03)00102-1.
- Zaki, M. F.; Elmaghraby, E. K. and Elbasaty, A. B. (2016). Structural alterations of polycarbonate/PBT by gamma irradiation for high technology applications. *Journal of adhesion science and Technology* 30(4): 443–457. Doi:10.1080/01694243.2015.1105123.
- Zaki, M. F. and Elmaghraby E. K. (2008). Photoluminescence of irradiation induced defects on CR-39. *Philosophical Magazine.* 88, 23, 11: 2945–2951. Doi: 10.1080/14786430802447052.
- Zhou, D.; Semones, E.; Mark, D. Weyland and Benton, E. R. (2007). LET calibration for CR-39 detectors in different oxygen environments. *Radiat. Meas.*, 42(9): 1499–1506.